1.2 Biophysics-based Modeling and Simulation in Medical Imaging

Alfonso Caiazzo, Sarah Katz, and Karsten Tabelow

Modern image acquisition technologies allow clinicians to record detailed information not only on patient anatomy, but also related to biophysical processes, such as fluid and tissue mechanics water diffusion, and metabolic activities. Those data can support clinicians in the quantitative estimation of relevant biomarkers for identifying and staging pathologies, as well as non-invasive patient monitoring, making medical imaging a pillar of non-invasive clinical diagnostics.

This article focuses on three selected applications of mathematical methods in the context of medical imaging: the estimation of pressure-related biomarkers from tissue displacement data, the estimation of tissue properties from magnetic resonance imaging (MRI) images, and usage of computational fluid dynamics to quantify complex blood flow behavior in the aorta, to highlight how different biophysical models and suitable computational frameworks can be used to exploit the information contained in the available data.

Data assimilation for magnetic resonance elastography

Magnetic resonance elastography (MRE) is an imaging acquisition technique sensitive to tissue mechanical properties. During the examination, the living tissue undergoes a mechanical excitation (10–100 Hz) whose response is recorded via motion-sensitive (phase-contrast MRI) images, resulting in a three-dimensional displacement field on selected tissue regions. Combined with suitable physical models, these displacement data allow to obtain non-invasive estimates of tissue mechanical parameters.

Elastography has been widely used for the quantitative estimation of biomarkers (e.g., stiffness, tissue fluidity, viscoelasticity) related to different tissue pathologies, supporting the diagnosing and staging of diseases, such as cancer and fibrosis. This section discusses the applicability of elastography for quantifying an increase of brain intracranial pressure (ICP), i.e., the pressure of the cerebrospinal fluid (CSF) within the brain, a condition that might be responsible for different neurological diseases or cerebral damages. This application is particularly challenging, for at least two reasons. Firstly, data are only available on a portion of the domain (typically a thin slice of the brain), which does not necessarily include the regions where the pressure shall be quantified. Secondly, these data are limited to the displacement field, i.e., the pressure is not observed. These aspects make the application of standard variational frameworks unsuitable, due to the high dimension of the unknown state and to the absence of consistent boundary conditions for the state variables.

We address this *state estimation* combining the numerical solutions of suitable partial differential equations (PDEs) with an optimization problem solved on a low-dimensional space. Namely, assuming to be given a set of displacement data over a few slices of the computational domain – mimicking the setting of an MRE acquisition – our goals are to (i) reconstruct suitable displacement and pressure fields on the whole brain, and (ii) to provide quantitative estimation of the pressure difference between the ventricles and the outer domain [2].

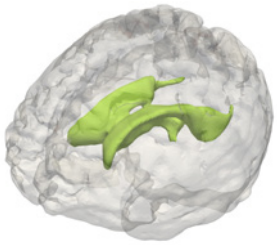

Fig. 1: Surface of the computational model including the outer CSF (gray) and the ventricles (green)

A computational model of a human brain was generated using full brain anatomical MRI images, segmented into a triangulated surface and filled with an unstructured tetrahedral mesh. Denoting with $\Omega \subset \mathbb{R}^3$ the resulting computational domain, the dynamics of the tissue is assumed to be described in terms of a displacement field $\mathbf{u} : \Omega \to \mathbb{R}^3$ and a pressure field $p : \Omega \to \mathbb{R}$ in a time interval $[0, T]$:

$$\begin{aligned} \rho\, \partial_{tt}\mathbf{u} - \boldsymbol{\nabla}\cdot\left(\frac{E}{1+\nu}(\nabla\mathbf{u} + \nabla\mathbf{u}^T)\right) + \nabla\cdot\frac{E\nu}{(1+\nu)(1-\nu)}\nabla\cdot\mathbf{u} + \boldsymbol{\nabla} p = 0 \quad \text{in } \Omega\times[0,T]\,, \\ S_\epsilon\,\partial_t p + \boldsymbol{\nabla}\cdot\partial_t\mathbf{u} - \frac{\kappa}{\mu}\nabla^2 p = 0 \quad \text{in } \Omega\times[0,T]\,. \end{aligned} \tag{1}$$

The system of PDE (1)[1] couples a linear, elastic solid phase with the motion of the fluid phase in the porous tissue. It depends on biophysical and mechanical parameters, such as tissue density (ρ), Young modulus (E), Poisson modulus (ν), tissue permeability (κ), fluid viscosity (μ), and mass-storage parameter (S_ϵ). Moreover, it depends on the boundary conditions to be imposed on the solid displacement and on the fluid pressure on the external and on the internal surfaces (the ventricles; see Figure 1).

The joint solution $v = (\mathbf{u}, p)$ is sought in a Hilbert *ambient* space V_h (e.g., piecewise linear finite elements for $\mathbf{u}$ and p), and we model the available measurements as m independent linear functionals $\ell_i : V_h \to \mathbb{R}$ $(i = 1, \dots, m)$, acting on the space V_h. In the target application, the images represent a three-dimensional displacement field on N_v voxels in the upper part of the brain, i.e., a total of $m = 3 \times N_v$ scalar measurements. As next, we construct an m-dimensional subspace that models how the solution is observed, as

$$W_m = \mathrm{Span}(w_i, \dots, w_m) \subset V_h\,, \tag{2}$$

spanned by the unique Riesz representers of the functionals ℓ_i, $i = 1, \dots, m$, i.e., such that it holds $\ell_i(v) = \langle w_i, v\rangle$, for all $v \in V_h$ and for all $i = 1, \dots, m$. The space W_m is also called the *space of observations*.

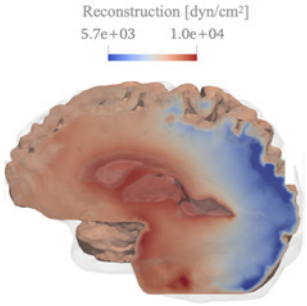

Fig. 2: Snapshot (cross section) of the reconstructed pressure field p^*, obtained solving (3)

We employ the physical model (1) to generate a *training set* $\mathcal{M}$, i.e., a manifold of solutions, by solving numerically (1) for different values of the biophysical parameters κ, E, ν, and $p_{\text{ventricles}}$ (CSF pressure at the ventricle boundary). The parameter ranges for the sampling can be chosen according to available literature, accounting automatically for parameter uncertainty. Moreover, including the pressure as parameter in the training set allows for considering different scenarios, such as distinguishing between healthy and increased pressure cases. As next, we compute an n-dimensional reduced-order subspace $V_n \subset V_h$ that approximates sufficiently well the training set $\mathcal{M}$ and whose dimension is much lower than the original ambient space (typically $n = O(10)$, while $\dim V_h = O(10^5)$). The space V_n encodes the physics of the model within the relevant parameter range, as it is spanned by solutions of system (1).

The considered state reconstruction problem reads: For a given set of observations $\hat{\lambda} \in \mathbb{R}^m$, find a state $v^* = (\mathbf{u}^*, p^*) \in V_h$, with

$$v^* = \mathrm{arginf}_{v\in V_h} \left\| v - \Pi_{V_n} v \right\|^2, \text{ with } \langle w_i, v\rangle = \hat{\lambda}_i,\ i = 1, \dots, m\,. \tag{3}$$

(Π_{V_n} stands for the orthogonal projection on V_n). Namely, we look for a solution in the whole space V_h that minimizes the distance from the V_n, i.e., $\left\| v - \Pi_{V_n} v \right\|$, but fits the available measurements.

Problem (3) can be formulated as a saddle-point problem of dimension $n+m$, whose well-posedness is ensured if $n \leq m$ and if the following condition is satisfied. The quantity $\beta(V_n, W_m)$ can be estimated numerically solving a singular value problem, and it can be seen as the *angle* between the reduced-order space V_n and the space of the observations W_m, and it quantifies the observability of the state with respect to the considered observation space.

$$\beta(V_n, W_m) := \inf_{v \in V_n} \frac{\|\Pi_{W_m} v\|}{\|v\|} > 0\,. \tag{4}$$

Figure 2 shows an example of the reconstructed pressure using partial displacement measurements, while Figure 3 shows the application for pressure increase characterization. Namely, the pressure difference between ventricle and outer CSF for reconstructed pressure p^* is used to assess whether it refers to a normal or to an increased pressure case. The algorithm is validated using synthetic measurements, comparing the classification to the one obtained using the true pressure field, showing that it is able to separate correctly the two regimes.

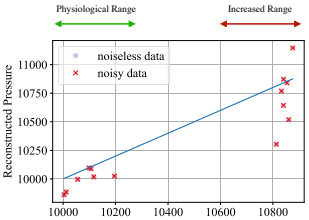

Fig. 3: *Characterization of normal and increased ventricle pressure, comparing the reconstructed and the synthetic true solutions*

Estimation of tissue parameters from inversion recovery MRI

Biological tissues are characterized by complex structures, whose dynamics reflects the interaction of fluid and solid compartments at very small spatial scales. Understanding this microscale properties is therefore of utmost importance in order to characterize mechanical and constitutive parameters that are used in tissue mechanical models at larger scales (e.g., the poroelastic models used in the previous section). Inversion recovery MRI (IRMRI) is an image acquisition technique that allows to obtain a time-dependent image intensity, sensitive to the presence of fluid in the tissue. This section focuses on mathematical methods to obtain improved tissue property estimation from brain IRMRI data, taking into account the inherent noise present in the images.

We consider a two-compartment model with a fluid and a solid phase. For each phase, the noise-free MR signal ξ depends on the time at which the sequence is acquired (the *inversion time*) and on the longitudinal relaxation rate $R_1 = 1/T_1$ (the reciprocal of the longitudinal relaxation time T_1) of the tissue within a voxel. In this simple model, the combined noise-free MR signal ξ can be described by a mixture model [3]

$$\xi(TI;\, f, I^f, R_1^f, I^s, R_1^s) = \Big|\, \underbrace{f I^f \left(1 - 2\mathrm{e}^{-TI\cdot R_1^f}\right)}_{\text{fluid contribution}} + \underbrace{(1-f) I^s \left(1 - 2\mathrm{e}^{-TI\cdot R_1^s}\right)}_{\text{solid contribution}} \Big|, \tag{5}$$

as a function of the inversion time TI, of the partial voxel volume containing the fluid phase f, and the parameters for the base signal intensity (I^f, I^s for fluid and solid, respectively) and the longitudinal relaxation rate in the fluid and solid phases (R_1^f and R_1^s, respectively). We distinguish between two main types of brain solid tissue, i.e., white and grey matter (WM and GM), while the fluid phase is constituted by the cerebrospinal fluid (CSF). The parameters related to the solid phase depend on the type of tissue (WM or GM). Furthermore, within the CSF, f is considered to be 1.

Parameter estimation of $\theta = (f, I^f, R_1^f, I^s, R_1^s)$ from available data is done by a quasi-likelihood estimation method. To this purpose, let $I(TI)$ denote the distribution of the MRI signal magnitude, and let σ denote the standard deviation of the noise. The rescaled magnitude $I(TI)/\sigma$ is assumed

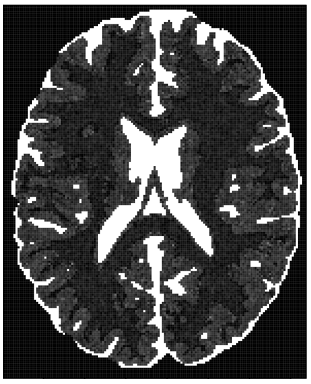

Fig. 4: *Results for smoothed estimated compartment parameter f for simulated data*

to be approximately χ-distributed with the non-centrality parameter ξ/σ and $2L'$ degrees of freedom. Estimates $\hat{\theta}$ can be obtained in each voxel relating the observed magnitude intensities $I(TI)$ with their expectations $\mu(\xi)$ by solving the optimization problem

$$\hat{\theta} = \arg\min_{\theta} \sum_i [I(TI_i) - \mu(\xi(TI_i, \sigma, L'; \theta)]^2 , \tag{6}$$

where $\mu(\xi) = \sigma\sqrt{\frac{\pi}{2}} L_{1/2}^{(L'-1)}\left(-\frac{\xi^2}{2\sigma^2}\right)$ is the expected value of signal distribution, and $L_{1/2}^{(L'-1)}$ is a generalized Laguerre polynomial. The analysis pipeline consists in the following steps (see Figure 4). Firstly, we segment the imaged brain tissue into the common three segments CSF, WM, and GM. Secondly, we estimate the parameters $\tilde{I}^f$ and $\tilde{R}_1^f$ for each voxel x within the CSF (using $f = 1$). Thirdly, we estimate $f(x)$, $I^s(x)$, and $R_1^s(x)$ in each voxel x of the GM and WM segments using model (5) and the parameters $\tilde{I}^f$ and $\tilde{R}_1^f$ from the previous step. Then, we perform local (adaptive) smoothing of $\tilde{I}(x)$ and $\tilde{R}_1(x)$ restricted to WM and GM (separately), to obtain estimates $\tilde{I}^s(x)$ and $\tilde{R}_1^s(x)$ with a reduced variance. Finally, the mixture parameter $f(x)$ of the model (5) is estimated again using the newly computed estimates $\tilde{I}^f$, $\tilde{R}_1^f$, $\tilde{I}^s(x)$, and $\tilde{R}_1^s(x)$.

Biomarkers estimation in blood flow

Aortic coarctation denotes a congenital heart condition characterized by the narrowing of a section of the aorta. The severity of the coarctation can be assessed using invasive measurement of the pressure gradient across the narrowed region. Non-invasive diagnosis based on medical imaging mainly consists in estimating the diameter of the narrowed area from anatomical data and the aortic pressure gradient from velocity images, e.g., acquired via cardiac MRI or ultrasound echocardiography. Other relevant biomarkers are related to abnormal flow conditions, such as increased flow asymmetries, and abnormal oscillatory behaviors of the wall shear stresses (WSS). Due to the limited resolution of image data, these quantities can only be quantified directly from medical imaging with reduced accuracy.

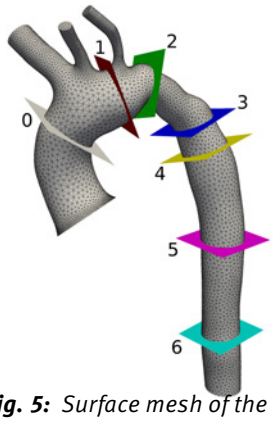

Fig. 5: *Surface mesh of the segment of aorta considered for the simulation. The cross sections were used to monitor averaged flow indicators.*

Computational hemodynamics plays an important role in supporting available medical data by performing patient specific simulations tuned to the particular physiological setting, which allows to obtain quantitative biomarkers estimations using anatomical images and flow data. The blood flow regime in the ascending aorta and the disturbances caused by aortic narrowing can yield to a transition to turbulence, which has to be properly taken into account in the computational model. The smallest scales of the turbulent dynamics cannot be neglected, for reasons of physical accuracy of the results, but full-scale numerical simulations of the whole scale spectrum are prohibitive. These challenges are addressed via *turbulence modeling*, i.e., with mathematical and numerical techniques to model the impact of the unresolved (small) scales onto the (large) resolved ones, so that important properties of the flow are preserved. The goal of this research is to study the impact of different turbulence modeling choices on selected quantities of interests, which are clinically relevant for the assessment of flow conditions in aortic coarctation [4].

Let $\Omega \subset \mathbb{R}^3$ denote a computational model of ascending and thoracic aorta, which can be obtained from medical images. The domain is bounded by the physical vessel wall Γ_{wall}, an inlet surface Γ_{in} – close to the left ventricle – and four outlet surfaces $\Gamma_{\text{out},i}$, $i = 1, 2, 3, 4$ (brachiocephalic, left common carotid, and left subclavian arteries, and downstream descending aorta), see Figure 5. The

blood flow in Ω is modeled as an incompressible, Newtonian fluid, whose dynamics is described in terms of a velocity field $\mathbf{u} : \Omega \to \mathbb{R}^3$ and a pressure field $p : \Omega \to \mathbb{R}$ satisfying, in a given time interval $(0, T]$, the incompressible Navier–Stokes equations

$$\begin{aligned} \rho \partial_t \mathbf{u} - 2\mu \nabla \cdot \mathbb{D}(\mathbf{u}) + \rho(\mathbf{u} \cdot \nabla)\mathbf{u} + \nabla p &= \mathbf{0} \quad \text{in } (0, T] \times \Omega, \\ \nabla \cdot \mathbf{u} &= 0 \quad \text{in } (0, T] \times \Omega. \end{aligned} \tag{7}$$

In (7), ρ stands for the blood density, μ is the blood dynamic viscosity, and $\mathbb{D}(\mathbf{u}) = \left(\nabla \mathbf{u} + (\nabla \mathbf{u})^T\right)/2$ denotes the velocity deformation tensor (i.e., the symmetric part of the velocity gradient). Boundary conditions for equations (7) are imposed using a measured inlet velocity profile on Γ_{in} and a resistive Neumann-type boundary condition on the outlet boundaries, of the form

$$P_i(t) = R_i \int_{\Gamma_{\text{out},i}} \mathbf{u} \cdot \mathbf{n} \, \mathrm{d}\mu_{\Gamma_{\text{out},i}}, i = 1, \ldots, 4, \tag{8}$$

where $\mathbf{n}$ stands for the outgoing normal vector. Equation (8) relates the boundary pressures to the outgoing fluxes via resistance parameters $R_1, \ldots R_4$, which model the resistance of the downstream circulation. The R_i are estimated to match observed systolic flow rates through each outlet.

Equations (7) and the boundary conditions are discretized using finite element spaces $\mathbf{V}_h$ and Q_h for velocity and pressure, introducing the variational form

$$\begin{aligned} A\left((\mathbf{u}_h, p_h), (\mathbf{v}_h, q_h)\right) :=& 2\nu \left(\mathbb{D}(\mathbf{u}_h), \mathbb{D}(\mathbf{v}_h)\right) + \left((\mathbf{u}_h \cdot \nabla)\mathbf{u}_h, \mathbf{v}_h\right) \\ &- \left(\nabla \cdot \mathbf{v}_h, p_h\right) + \left(\nabla \cdot \mathbf{u}_h, q_h\right) - f(\mathbf{u}_h, \mathbf{v}_h) \end{aligned} \tag{9}$$

(where $f(\mathbf{u}_h, \mathbf{v}_h)$ contains the outflow boundary condition terms), and solving the problem: Find $(\mathbf{u}_h, p_h) : [0, T] \to \mathbf{V}_h \times Q_h$, satisfying the initial and the boundary conditions, such that

$$\left(\partial_t \mathbf{u}_h, \mathbf{v}_h\right) = -A\left((\mathbf{u}_h, p_h), (\mathbf{v}_h, q_h)\right), \text{ for all } t \in (0, T) \text{ and for all } (\mathbf{v}_h, q_h) \in \mathbf{V}_h \times Q_h. \tag{10}$$

We consider then two types of turbulence models. The first class are *Large Eddy Simulation* (LES) methods, such as the original Smagorinsky model, the Vreman model, and the more recent σ -model. These attempt to model the large turbulent scales surrogating the effect of the small scales into explicit models for the stress tensor. In this case, the bilinear form (9) is modified as

$$\hat{A}_\theta\left((\mathbf{u}_h, p_h), (\mathbf{v}_h, q_h)\right) = A\left((\mathbf{u}_h, p_h), (\mathbf{v}_h, q_h)\right) + \left(\nu_t \, \mathbb{D}(\mathbf{u}_h), \mathbb{D}(\mathbf{v}_h)\right), \tag{11}$$

where ν_t denotes the *eddy viscosity*, i.e., additional modeled dissipation due to the smallest, not resolved, scales, and θ stands for a set of model parameters to be properly chosen. A different approach is the *residual-based variational multiscale method* (RB-VMS), which is based on a two-scale decomposition of the analytic function spaces for velocity and pressure, surrogating the influence of the small scales into additional terms in the finite element formulation. For the RB-VMS, the bilinear form (9) is modified taking into account the momentum residue of the coarse scale solution.

Figure 6 shows a snapshot of the simulated blood flow for the σ -model. Depending on the considered biomarkers, the obtained results for different turbulence models are either quite similar (see Figure 7) or they are notably different. In summary, our results confirm that modeling and

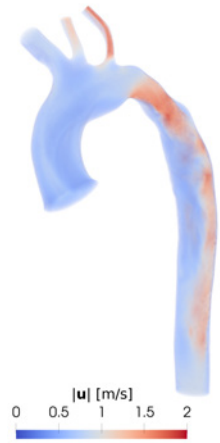

Fig. 6: *Snapshot of the numerical solution (velocity magnitude) at a selected instant, for the σ -turbulence model*

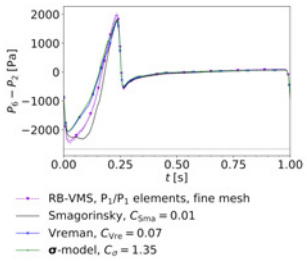

Fig. 7: *Pressure difference across the narrowing for different models, compared with critical value used in clinical assessment (dashed)*

discretization choices have an important impact on the time-dependent dynamics. An extension of this study to several non-Newtonian blood flow models can be found in [5].

Conclusions and outlook

In medical imaging, data quality and information density are closely linked. Increasing spatial resolution, for example, requires longer acquisition times, which in turn can lead to inaccuracies arising from intrinsic organ and patient motion. At WIAS, this research area is based on joint research activities across different research groups as well as with interdisciplinary collaborations with clinical and experimental partners, ensuring that the lines of research tackle relevant challenges, both from the mathematical and from the clinical perspectives.

This article showed few examples on how biophysics-based data assimilation approaches can compensate for the limited availability of data by combining the available data with advanced mathematical models, numerical methods, and efficient algorithms. In the first example, reduced-order modeling and linear poroelasticity were used to reconstruct a full solution of an unknown pressure field using limited displacement data. The second example showed how statistical image intensity models can be used to exploit the influence of tissue properties, such as porosity, on tissue image intensity. The last example focused on the impact of different choices for turbulence modeling in the context of patient-specific modeling of aortic coarctation. Future directions will explore how these approaches can be used not only to enhance the physical consistency and clinical relevance of imaging data, but also to support long-term prediction in conjunction with follow-up imaging examination.

References

[1] M. Biot, D. Willis, *The elastic coefficients of the theory of consolidation*, J. Appl. Mech., **15** (1957), pp. 594–601.

[2] F. Galarce, K. Tabelow, J. Polzehl, C.Panagiotis Papanikas, V. Vavourakis, L. Lilaj, I. Sack, A. Caiazzo, *Displacement and pressure reconstruction from magnetic resonance elastography images: Application to an in silico brain model*, WIAS Preprint no. 2933, 2022, in press in: SIAM J. Imaging Sci.

[3] L. Lilaj, H. Herthum, T. Meyer, M. Shahryari, G. Bertalan, A. Caiazzo, J. Braun, T. Fischer, S. Hirsch, I. Sack, *Inversion-recovery MR elastography of the human brain for improved stiffness quantification near fluid-solid boundaries*, Magn. Reson. Med., **86**:5 (2021), pp. 2552–2561.

[4] S. Katz, A. Caiazzo, B. Moreau, U. Wilbrandt, J. Brüning, L. Goubergrits, V. John, *Impact of turbulence modeling on the simulation of blood flow in aortic coarctation*, 2022, Int. J. Numer. Methods Biomed. Engng. 2023, pp. e3695/1–e3695/36.

[5] S. Katz, A. Caiazzo, V. John, *Impact of viscosity modeling on the simulation of aortic blood flow*, J. Comput. Appl. Math., **425** (2023), pp. 115036/1–18.